Inertial-confinement fusion-plasma-based cross-calibration of the deuterium-tritium γ-to-neutron branching ratio

J. Jeet,[1,*] A. B. Zylstra,[1] M. Rubery,[1] Y. Kim,[2] K. D. Meaney,[2] C. Forrest,[3] V. Glebov,[3] C. J. Horsfield,[4] A. M. McEvoy,[2] and H. W. Herrmann[2]

[1]*Lawrence Livermore National Laboratory, Livermore, California 94550, USA*
[2]*Los Alamos National Laboratory, Los Alamos, New Mexico 87545, USA*
[3]*Laboratory for Laser Energetics, Rochester, New York 14623, USA*
[4]*Atomic Weapons Establishment, Aldermaston, Reading, Berkshire RG7 4PR, England, United Kingdom*

(Received 25 August 2021; accepted 21 October 2021; published 29 November 2021)

The deuterium-tritium (D-T) γ-to-neutron branching ratio [^{3}H$(d,\gamma)^5$He / ^{3}H$(d,n)^4$He] has been determined previously under inertial-confinement fusion (ICF) conditions and in beam-target based experiments. In the former case, neutron-induced backgrounds are mitigated compared to the latter due to the short pulse nature of ICF implosions and the use of gas Cherenkov γ-ray detectors. An added benefit of ICF based measurements is the ability to achieve lower center-of-mass energies as compared to accelerators. Previous ICF based experiments however report a large uncertainty in the D-T γ-to-neutron branching ratio of $\approx$48%, which arises from the necessity of an absolute detector calibration and/or a cross-calibration against the D-^{3}He γ-to-proton branching ratio. A more precise value for the branching ratio based on data taken at the OMEGA laser facility is reported here, which relies on a cross-calibration against the better known ^{12}C neutron inelastic scattering cross section. A D-T branching ratio value of $(4.6 \pm 0.6) \times 10^{-5}$ is determined by this method.

DOI: 10.1103/PhysRevC.104.054611

I. INTRODUCTION

A. D-T nuclear fusion

The deuterium-tritium (^{2}H-^{3}H or D-T) reaction,[1] with resonance at $\approx$100 keV, has been extensively studied and is known to have the largest fusion cross section at center-of-mass energies below 500 keV. ^{3}H$(d,n)^4$He is the neutron producing branch of the D-T reaction, while ^{3}H$(d,\gamma)^5$He is the γ producing branch which occurs much less frequently than the former. The ^{3}H$(d,n)^4$He reaction, shown in Eq. (1), results in the production of a 14.1-MeV neutron and a 3.5-MeV alpha particle. Equations (2) and (3) represent the ^{3}H$(d,\gamma)^5$He reaction in which an excited ^{5}He nucleus relaxes via γ emission. Upon relaxation to its ground state, a 16.75-MeV γ ray (γ_0) is emitted, represented by Eq. (2). In Eq. (3), an excited ^{5}He nucleus relaxes to its first excited state, resulting in a broad γ emission line (γ_1) with peak at $\approx$13.5 MeV:

$$\mathrm{D} + \mathrm{T} \rightarrow {}^5\mathrm{He}^* \rightarrow {}^4\mathrm{He}(3.5\,\mathrm{MeV}) + n(14.1\,\mathrm{MeV}), \quad (1)$$

$$\mathrm{D} + \mathrm{T} \rightarrow {}^5\mathrm{He}^* \rightarrow {}^5\mathrm{He} + \gamma_0(16.75\,\mathrm{MeV}), \quad (2)$$

$$\mathrm{D} + \mathrm{T} \rightarrow {}^5\mathrm{He}^* \rightarrow {}^5\mathrm{He}^* + \gamma_1(\approx 13.5\,\mathrm{MeV}). \quad (3)$$

The D-T γ-to-neutron (γ/n) branching ratio, [^{3}H$(d,\gamma)^5$He / ^{3}H$(d,n)^4$He], is of fundamental interest from a nuclear and plasma physics perspective [1–2]. Constraining its value is of great relevance to experimental efforts at inertial-confinement facilities and magnetic confinement facilities. Accurate measurements of the D-T reaction fusion products, enabled by a host of diagnostics, are necessary to assess and characterize performance. For tokomak-based nuclear reactors, such as JET and ITER, determination of the power gain factor (Q) is essential. In addition to neutron diagnostics [3–4], a direct measurement of D-T fusion γ's along with a precise value of the D-T (γ/n) branching ratio can augment and potentially facilitate the measurement of Q. This is motivated by the fact that the D-T γ's will be less perturbed by structural features as compared to the neutrons, and the γ spectrum is distinct from other neutron scattering sources. At inertial-confinement fusion (ICF) facilities, the D-T branching ratio can provide absolute yield measurements based on γ-ray diagnostics.

B. D-T fusion at inertial-confinement fusion facilities

The 192 beam National Ignition Facility (NIF) in Livermore, California is the world's most energetic ICF facility [5]. The primary goal at the NIF is to achieve self-sustaining fusion burn, by utilizing its high energy lasers (up to 1.8 MJ) to implode capsules containing D-T fuel. The NIF and other ICF facilities, such as the OMEGA Laser Facility at the Laboratory for Laser Energetics in Rochester, New York [6], also provide a platform to conduct experiments which are crucial for diagnosing aspects of implosion physics [7–10] and for studying nuclear reactions [11–15]. The application

*jeet1@llnl.gov

[1]Throughout the paper we use the conventional abbreviations D for ^{2}H and T for ^{3}H.

of terawatt laser power onto spherical targets will cause the outer part of the capsule shell to heat up and ionize. As the outer part of the shell explodes, the inner part is accelerated toward the center of the sphere to conserve momentum. The gaseous D-T fuel is compressed, ionized, and heated up to thermonuclear fusion temperatures in this process [5,16]. To realize ignition, understanding the fusion reaction history is necessary to assess the quality of the implosion [17–18]. This can be achieved through characterization of the D-T fusion products. Because γ rays do not Doppler broaden in transit, as compared to neutrons, γ-ray diagnostics can be advantageous in determining a fusion reaction history. A precise value of the D-T (γ/n) branching ratio would enable absolute yield measurements from γ-ray detectors, which at ICF facilities are primarily based on the Cherenkov mechanism [19].

C. Cherenkov γ-ray detectors

ICF facilities currently utilize Cherenkov radiators for both neutron and γ-ray detection. Fused silica is used as a radiator for γ-ray detection in both the neutron time-of-flight (nToF) quartz Cherenkov detectors at the NIF [20–21], and the Diagnostic for Areal Density (DAD) at OMEGA [22]. Gaseous media are used for the gamma reaction history (GRH) and gas Cherenkov detectors (GCD-1, -2, and -3) [23–24]. In a Cherenkov radiator, relativistic electrons produced through the Compton scattering of γ's produce photons at ultraviolet and visible wavelengths via the Cherenkov effect [19]. In this mechanism, atomic electrons in the propagation medium absorb the field energy of the relativistic electrons and radiate photons. The energy emitted due to any relativistic charged particle can be described by the Frank-Tamm formula shown in Eq. (4). Here q is the charge of the particle, ω is the emitted photon frequency, $\mu(\omega)$ is the electromagnetic permeability, and $n(\omega)$ is the index of refraction. For Cherenkov photon generation at frequency ω, $\beta = v/c > 1/n(\omega)$, where v is the speed of the charged particle in the medium and c is the speed of light in vacuum. Combining this requirement with the relativistic kinetic energy of an electron results in Eq. (5). This describes the electron energy threshold for Cherenkov photon production. Here m_e is the mass of the electron. It can be seen that as the index of refraction of an optically transmissive medium is increased, the electron energy threshold will decrease:

$$\frac{d^2E}{dxd\omega} = q^2\mu(\omega)\omega\left\{1 - \frac{c^2}{v^2n^2(\omega)}\right\}, \tag{4}$$

$$E_{\text{threshold}} = m_ec^2\left\{\frac{1}{\sqrt{1 - n^{-2}}} - 1\right\}. \tag{5}$$

For gas-based Cherenkov detectors, the gas composition and pressure will affect the index of refraction and therefore the electron energy threshold [23]. See Fig. 1 for an illustrated schematic of the GCD. γ's can Compton scatter in a converter disk which is typically aluminum or beryllium. The resulting relativistic electrons can generate Cherenkov photons as they propagate through the gas medium. These photons are guided by a Cassegrainian mirror setup to a microchannel-plate photomultiplier tube (PMT) for detection.

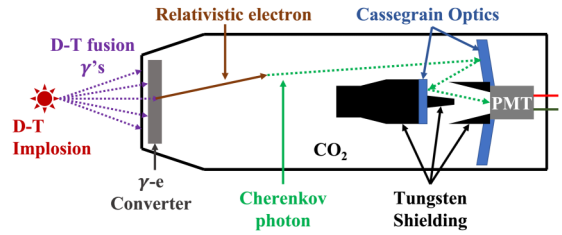

FIG. 1. An illustrated schematic of the GCD. D-T fusion γ's Compton scatter in the γ-e converter plate to produce relativistic electrons. The relativistic electrons generate Cherenkov radiation as they propagate through the gas medium inside the GCD. The resulting Cherenkov photons are reflected by a Cassegrainian mirror setup to a PMT for detection. Tungsten shielding is used to attenuate γ's which can directly interact with the PMT to produce an extraneous signal. The distance between the pair of mirrors in the Cassegrainian setup provides a temporal delay between Cherenkov photon detection and direct γ interactions in the PMT.

Tungsten shielding is used to attenuate γ's which can directly interact with the PMT to create an extraneous signal. The Cassegrainian mirror setup also serves to temporally delay the primary Cherenkov signal from the extraneous γ signal. For absolute measurements of the fusion reaction history, as well as in determination of nuclear physics cross sections, a calibration of the diagnostic is required. This can be achieved either through a cross-calibration against a highly accurate neutron yield measurement, or the precise D-T (γ/n) branching ratio.

D. Previous research on the D-T (γ/n) branching ratio

There have been extensive efforts to measure the D-T (γ/n) branching ratio, $[^3\text{H}(d,\gamma)^5\text{He}\,/\,^3\text{H}(d,n)^4\text{He}]$. Measurements have been made via accelerator-based beam-target experiments [25–32], as well as under ICF conditions [11–12]. There is significant discrepancy in the obtained results. This can be attributed to the relatively small value of the D-T (γ/n) branching ratio, uncertainties in the γ-ray emission spectrum [31,33], as well as the large background noise that can be produced by neutron scattering. In accelerator-based experiments, a deuteron beam is typically incident on a tritium-based target with corresponding center-of-mass energies which are typically greater than values relevant for fusion plasmas ($\gtrsim$100 keV). Scintillator detectors are placed at different angles and distances from the target. Techniques employing time-of-flight configurations, coincidence counting, pulse-shape discrimination, shielding and collimation, and pulsed deuteron sources can help to mitigate neutron-induced noise [31].

At ICF facilities, the fusion products are inherently intense and extremely short in duration. Neutron yields can reach an excess of 10^{16} with burn widths typically less than 200 ps. Nuclear diagnostics are essential in diagnosing the fusing plasmas. Multiple nToF detectors, the magnetic recoil spectrometer [34], and neutron activation diagnostics [35] are used in conjunction to accurately determine the neutron yields. The γ-ray yields are determined with the GRH and GCD, typically operated at various gas pressures.

In a single shot ICF experiment, undesired neutron-induced backgrounds can be eliminated through high-bandwidth electronics by temporally separating the D-T fusion γ rays. In previous ICF experiments to determine the D-T (γ/n) branching ratio [11–12], two different methods were utilized. The first involved a direct measurement of ICF D-T γ-ray and neutron emissions using absolutely calibrated detectors including GCD-1, and the second involved a separate cross-calibration against the D-^{3}He γ-to-proton (γ/p) branching ratio [^{3}He(d,γ) ^{5}Li / ^{3}He(d,p) ^{4}He]. In the former scenario, the D-T branching ratio is reported to be $(4.3 \pm 1.8) \times 10^{-5}$ with a 7.3% statistical uncertainty and 33.9% systematic uncertainty. In the latter scenario involving the cross-calibration to the D-^{3}He γ-to-proton (γ/p) branching ratio, the D-T branching ratio is reported to be $(3.9 \pm 2.3) \times 10^{-5}$ with a 25.4% statistical uncertainty and 33.6% systematic uncertainty. The variance weighted value for the two methods is $(4.2 \pm 2.0) \times 10^{-5}$. This paper is an extension of these experiments and involves a cross-calibration against the inelastic neutron scattering cross section in ^{12}C**,** the ^{12}C$(n,n'\gamma)$ ^{12}C reaction. The primary advantage of using this reaction is that the cross section has been recently reevaluated, described in the following section, and is known to significantly greater precision than the D-^{3}He (γ/p) branching ratio. By measuring both the D-T fusion and ^{12}C γ's resulting from the ^{12}C$(n,n'\gamma)$ ^{12}C reaction, in a single shot D-T implosion, absolute detector calibrations of the GCD-3 and PMT are obviated. The details of the experiment and the method used will be described in more detail in subsequent sections.

II. THE D-T (γ/n) BRANCHING RATIO VIA A CARBON CROSS-CALIBRATION

A. The ^{12}C$(n,n'\gamma)$ ^{12}C spectrum and cross section

Cockcroft-Walton accelerators have often been used in past experiments to generate a deuteron beam. In addition to studying D-T fusion, impingement of a deuteron beam on a target containing tritium can serve as a source of 14.1-MeV neutrons. Several experiments conducted in the past have utilized this method to investigate the inelastic neutron scattering cross section in ^{12}C, or the ^{12}C$(n,n'\gamma)$ ^{12}C reaction. The neutron-induced γ-ray spectrum from ^{12}C is shown in Fig. 2 [36–37] and has an intense peak at 4.44 MeV. This feature is orders of magnitude more intense than other features in the spectrum, making it approximately monoenergetic.

To accurately define the ^{12}C$(n,n'\gamma)$ ^{12}C cross section for 14.1-MeV neutrons, the results from a few experiments conducted in the past [37–39], in which the angle (θ) between the incident neutron and measured γ is varied, are used to determine a single adopted differential cross section [40]. A total cross section is calculated from the adopted differential cross section and is reported to be 217.5 ± 5.5 mb according to Ref. [40]. The inelastic neutron scattering cross section in ^{12}C is one of the largest known cross sections, and the resulting γ emission spectrum is distinct. These factors facilitate experimental efforts that rely on the ^{12}C$(n,n'\gamma)$ ^{12}C reaction. This comprehensive evaluation of the cross section for ^{12}C$(n,n'\gamma)$ ^{12}C [40] is essential for a cross-calibration of the D-T (γ/n) branching ratio.

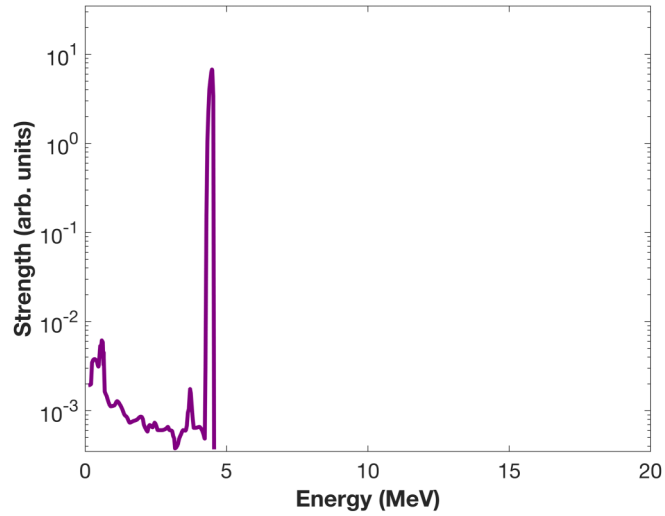

FIG. 2. The ^{12}C$(n,n'\gamma)$ ^{12}C spectrum [36–37] resulting from 14.1-MeV neutrons. The spectrum is approximately monoenergetic due to the intense line at 4.4 MeV which is orders of magnitude larger than other spectral features.

B. Experimental setup and data

ICF implosions were conducted at the University of Rochester OMEGA Laser Facility [6]. The experiment utilizes 60 laser beams, at 351 nm, with a square pulse of 1 ns in duration and total energy of $\approx$27 kJ. The targets are SiO_2 shells of $\approx$3.7 μm in thickness and with outer diameters ranging from 874.4 to 881.2 μm. The shells are filled with 10 atm of gaseous, equimolar D-T fuel. The front face of the GCD-3 is located 20 cm from the target chamber center (TCC). A beryllium puck holder extends from the GCD-3 such that its inner, front face is 6.26 cm from TCC [41]. See Fig. 3.

The puck holder has an inner diameter of 2.709 cm and a depth of 0.914 cm. For the relevant experimental shots, the puck holder is either filled with ^{12}C powder (with a total mass of 5.93 $\pm$ 0.1 g) or is empty. In the former case or active configuration, the 14.1-MeV D-T fusion neutrons can inelastically scatter in the ^{12}C puck to produce 4.4-MeV γ's. Because the neutrons can also scatter in other structural components to produce γ's, the latter case (background configuration) provides a neutron-induced background measurement for comparison. The experimental setup enables the D-T fusion γ rays to arrive at the detector $\approx$1 ns prior to the neutron-induced γ rays, due to the flight time of the 14.1-MeV neutrons and the distance to the beryllium puck holder and other structural features. The GCD-3 is operated with CO_2 gas at a pressure of 400 psi (absolute), corresponding to an electron threshold energy of $\approx$2.6 MeV. A PMT, Photek PMT110, with a fast temporal response is used for the detection of Cherenkov photons.

The scope traces from four different shots, which were conducted under similar experimental conditions, are shown

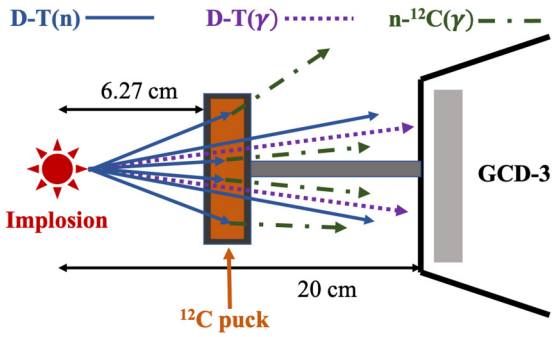

FIG. 3. The GCD-3 and ^{12}C puck experimental configuration [41]. The inner, front face of the beryllium puck holder is 6.26 cm from TCC. The front face of the GCD-3 is 20 cm from TCC. D-T fusion neutrons (solid, blue arrows) can inelastically scatter in the ^{12}C puck to generate ^{12}C γ's (dot-dashed, green arrows). The D-T fusion γ's (dotted, purple arrows) are mostly unattenuated by the beryllium puck holder and ^{12}C puck. The experimental layout allows the fusion γ's to arrive at the GCD-3 $\approx$1 ns before the arrival of neutron-induced γ's.

in Fig. 4. These traces are normalized to the product of the D-T fusion neutron yield, photomultiplier tube gain, and mean quantum efficiency over the Cherenkov spectrum. Shot numbers 77 361 and 77 374 correspond to experiments conducted with the ^{12}C puck (active configurations), while 77 365 and 77 367 were conducted with an empty beryllium puck holder (background configurations). The scope traces have been shifted such that the D-T fusion γ peaks coincide with

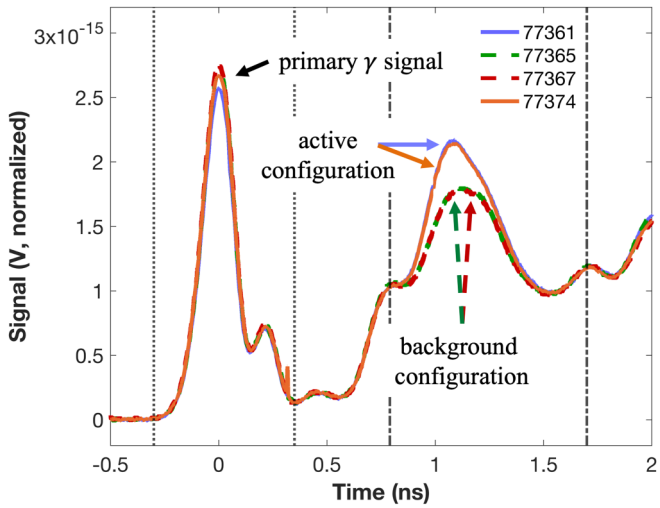

FIG. 4. Scope traces from four different shots. These traces are normalized to the product of the D-T neutron yield, photomultiplier tube gain, and mean quantum efficiency over the Cherenkov spectrum. Shots 77 361 and 77 374 (blue and orange, solid lines) are in the active configuration in which the beryllium puck holder is loaded with the ^{12}C powder. Shots 77 365 and 77 367 (green and red, dashed lines) are in the background configuration in which the beryllium puck holder is empty. An excess signal can be seen from 0.8 to 1.6 ns in the active configuration which is due to ^{12}C$(n, n'\gamma)$ ^{12}C and subsequent ^{12}C γ detection by the GCD-3.

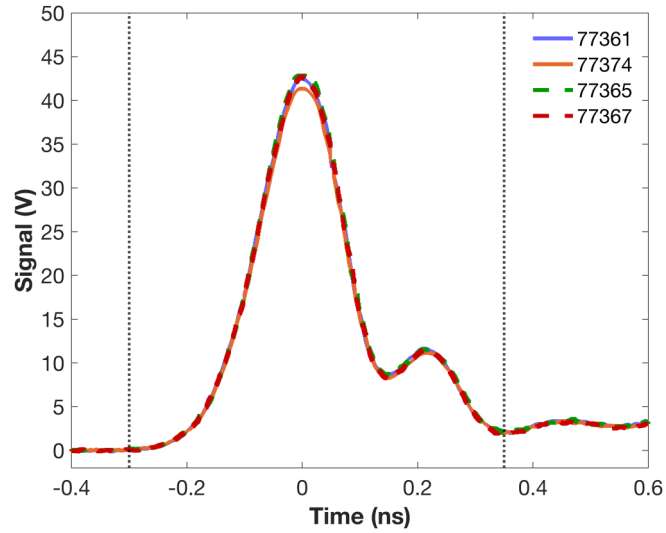

FIG. 5. The D-T fusion γ signal. This signal is representative of the raw (non-normalized) signals shown in Fig. 4. The initial peak at $t = 0$ is a result of peak emission of D-T fusion γ's during the implosion. The second peak near 200 ps is due to ringing and is inherent to the instrument response function of the Photek PMT110.

$t = 0$ with the dotted, vertical lines representing the beginning and end of the D-T fusion γ signal. The dot-dashed, vertical lines represent the beginning and end of the ^{12}C γ signal. There is an excess signal in this region for the active configurations. The un-normalized D-T fusion γ signals are shown in Fig. 5. The initial peak at $t = 0$ results from peak emission of γ's during the implosion. The second peak near 200 ps is an artifact of ringing and is inherent to the instrument response function of the Photek PMT110. The ^{12}C γ signal in the active configurations can be isolated from the extraneous neutron-induced noise through subtraction of the normalized background configuration traces. The resulting traces are then renormalized to the appropriate D-T neutron yield, PMT gain, and mean quantum efficiency. The results are shown in Fig. 6. The extraction of a clean ^{12}C$(n, n'\gamma)$ ^{12}C γ signal, along with the reevaluated cross section, permits the experimental determination of the D-T (γ/n) branching ratio using a cross-calibration method.

C. The cross-calibration method

The integral of the D-T fusion γ signal, shown in Fig. 5, can be expressed as

$$S_\gamma^{\mathrm{DT}}(E_{\mathrm{thr}}) = Y_\gamma^{\mathrm{DT}} \times \left(\frac{\Delta\Omega_\gamma^{\mathrm{DT}}}{4\pi}\right) \times QGer \times \int_{E_{\mathrm{thr}}}^{\infty} I_\gamma^{\mathrm{DT}}(E) R'(E, E_{\mathrm{thr}}) dE. \quad (6)$$

Here Y_γ^{DT} is the D-T fusion γ yield and $\Delta\Omega_\gamma^{\mathrm{DT}}/4\pi$ is the solid angle fraction for the collection of fusion γ's by the GCD-3. Q is the mean quantum efficiency of the PMT over the Cherenkov spectrum, G is the PMT gain, e is the charge of an electron, and r is the input impedance of the

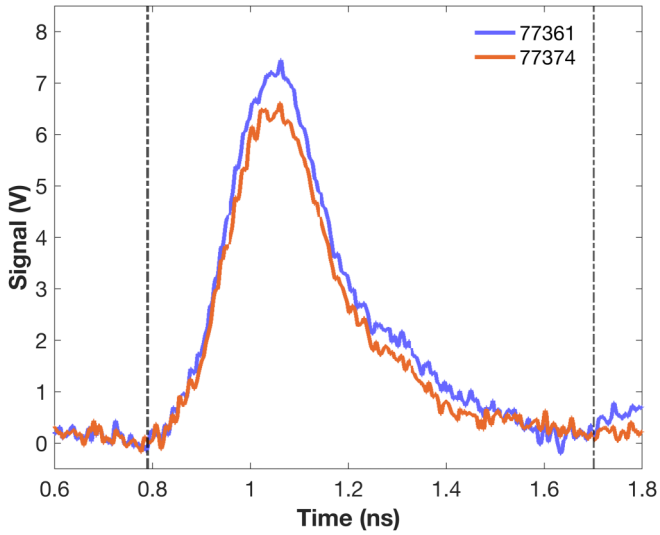

FIG. 6. The ^{12}C γ signal. The signal results from the normalized traces shown in Fig. 4. The background configuration shot trace is subtracted from the active and the result is renormalized to the appropriate neutron yield, PMT gain, and quantum efficiency.

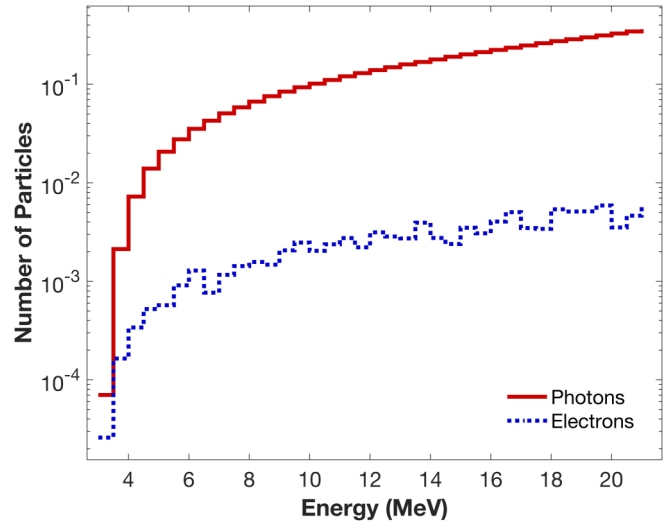

FIG. 7. The GCD-3 responsivity, in productive particles per incident γ for 400 psi (absolute) of CO_2, is determined from Monte Carlo simulations conducted in GEANT4. The solid, red curve is representative of photons and the dotted, blue curve denotes electrons.

digitizer or scope used in the data acquisition. $I_\gamma^{\rm DT}(E)$ is the D-T γ spectrum and $R'(E, E_{\rm thr})$ is the GCD-3 responsivity in Cherenkov photons collected per incident γ. The D-T γ spectrum is based on R-matrix analysis [42] of neutron-alpha particle scattering which predicts the existence and shape of the D-T $\gamma_0(E)$ and $\gamma_1(E)$ spectral features, but not their relative strengths. D-T implosions were conducted at OMEGA with γ measurements taken by the GCD-1 at various threshold energies [33]. The experiments report an optimal $\gamma_1 : \gamma_0\,(Gr)$ ratio of $(2.1 \pm 0.4) : 1$. An appropriate expression for the resulting area-normalized spectral shape is given by

$$I_\gamma^{\rm DT}(E) = \frac{\gamma_0(E) \; + \; [Gr \; \times \; \gamma_1(E)]}{1 \; + \; Gr}. \tag{7}$$

The GCD-3 responsivity $[R'(E, E_{\rm thr})]$ for 400 psi (absolute) of CO_2 is shown in Fig. 7. This is based on GEANT4 Monte Carlo simulations [43].

In Eq. (6), the D-T γ yield can be replaced with the product of the neutron yield $(Y_n^{\rm DT})$, which is measured to high accuracy in ICF implosions, and the D-T (γ/n) branching ratio $(B_{\frac{\gamma}{n}}^{\rm DT})$:

$$S_\gamma^{\rm DT}(E_{\rm thr}) = Y_n^{\rm DT} \times B_{\frac{\gamma}{n}}^{\rm DT} \times QGer \times \left(\frac{\Delta\Omega_\gamma^{\rm DT}}{4\pi}\right) \times \int_{E_{\rm thr}}^{\infty} I_\gamma^{\rm DT}(E) R'(E, E_{\rm thr}) dE. \tag{8}$$

The resulting expression can be solved for the branching ratio:

$$B_{\frac{\gamma}{n}}^{\rm DT} = \frac{S_\gamma^{\rm DT}(E_{\rm thr})}{QGer\left(\frac{\Delta\Omega_\gamma^{\rm DT}}{4\pi}\right)} \frac{1}{Y_n^{\rm DT} \int_{E_{\rm thr}}^{\infty} I_\gamma^{\rm DT}(E) R'(E, E_{\rm thr}) dE}. \tag{9}$$

The expression in Eq. (9) represents a direct measurement of the D-T (γ/n) branching ratio. It requires an absolute calibration of the detector used for Cherenkov photon detection. The gain and quantum efficiency of PMT's are susceptible to temperature fluctuations and can degrade over time. For these reasons, a cross-calibration can be desirable which removes any uncertainty in the PMT response and obviates the absolute calibration of the detector. For the ^{12}C puck used in the experiments, the areal density $(\langle \rho_{\rm C} R \rangle_{\rm puck})$ is equal to $\rho_{\rm C} T$, where $\rho_{\rm C}$ is the ^{12}C powder density and T is the puck thickness. The product of the areal density and solid angle fraction for 14.1-MeV neutron collection by the puck $(\Delta\Omega_n^{\rm puck}/4\pi)$ is equivalently expressed as

$$\langle \rho_{\rm C} R \rangle_{\rm puck} \times \left(\frac{\Delta\Omega_n^{\rm puck}}{4\pi}\right) = \frac{M_{\rm puck}}{4\pi D^2}. \tag{10}$$

Here $M_{\rm puck}$ is the total ^{12}C puck mass and D is its distance to TCC. The ^{12}C γ yield is given by

$$Y_\gamma^{\rm puck} = \left(\frac{\Delta\Omega_n^{\rm puck}}{4\pi}\right) \times Y_n^{\rm DT} \times \frac{\sigma_{n{\rm C,total}}}{m_{\rm C}} \times \langle \rho_{\rm C} R \rangle_{\rm puck}. \tag{11}$$

$\sigma_{n{\rm C,total}}$ is the total inelastic neutron scattering cross section calculated in Ref. [40], and $m_{\rm C}$ is the mass of a ^{12}C atom. The integral of the ^{12}C γ signal shown in Fig. 6 can be expressed as

$$S_\gamma^{\rm puck} = QGer \times Y_n^{\rm DT} \times \frac{\sigma_{n{\rm C}}}{m_{\rm C}} \times f_1 \times \left(\frac{M_{\rm puck}}{4\pi D^2}\right) \times \left(\frac{\Delta\Omega_\gamma^{\rm puck}}{4\pi}\right) \times \int_{E_{\rm thr}}^{\infty} I_\gamma^{\rm puck}(E) R''(E, E_{\rm thr}) dE. \tag{12}$$

$\sigma_{n{\rm C}}$ here is the inelastic neutron scattering cross section at $\theta = 90°$, and f_1 is a geometrical efficiency factor which accounts for the scattering angles from the ^{12}C puck which result in γ's incident on the GCD-3 [40,44]. This is calculated in Ref. [40] by integrating the normalized differential scattering cross section $[\sigma(\theta)/\sigma(90°)]$ over the appropriate

range of angles. The resulting value for f_1 is 1.369 ± 0.089. $\Delta\Omega_\gamma^{\text{puck}}/4\pi$ is the GCD-3 solid angle fraction for collection of ^{12}C γ's and $I_\gamma^{\text{puck}}(E)$ is the ^{12}C$(n,n'\gamma)$ ^{12}C γ spectrum shown in Fig. 2. It should be noted that $R''(E, E_{\text{thr}})$ in Eq. (12) is not equivalent to $R'(E, E_{\text{thr}})$ in Eq. (6). The latter corresponds to the GCD-3 responsivity to γ's emitted from TCC while the former responsivity is unique to the puck geometry and its distance to the GCD-3 front face.

With these definitions, the D-T (γ/n) branching ratio can be defined relative to the ^{12}C puck measurement. This is accomplished by taking the ratio of the signals given by the expressions in Eqs. (8) and (12) and solving for the branching ratio:

$$B_{\frac{\gamma}{n}}^{\text{DT}} = \frac{\Delta\Omega_\gamma^{\text{puck}} M_{\text{puck}}}{\Delta\Omega_\gamma^{\text{DT}} 4\pi D^2 m_C} \times \sigma_{nC} \times f_1 \times \left\{ \frac{S_\gamma^{\text{DT}}(E_{\text{thr}})}{S_\gamma^{\text{puck}}(E_{\text{thr}})} \right\} \times \left\{ \frac{\int_{E_{\text{thr}}}^{\infty} t_n^{\text{puck}} t_\gamma^{\text{puck}}(E) I_\gamma^{\text{puck}}(E) R''(E, E_{\text{thr}}) dE}{\int_{E_{\text{thr}}}^{\infty} t_\gamma^{\text{DT}}(E) I_\gamma^{\text{DT}}(E) R'(E, E_{\text{thr}}) dE} \right\} \tag{13}$$

The integrals over the ^{12}C$(n,n'\gamma)$ ^{12}C and D-T fusion γ spectra include additional terms accounting for the attenuation of neutrons and γ's in the beryllium puck holder and ^{12}C puck. t_n^{puck} is the transmission of 14.1-MeV neutrons through half of the puck holder and puck. This is determined in GEANT4 simulations to be 0.94. $t_\gamma^{\text{puck}}(E)$ is the energy-dependent transmission of γ's in half of the puck holder and puck. This is determined from bulk mass attenuation coefficients provided by NIST [45], for the appropriate materials. An integration of $t_\gamma^{\text{puck}}(E)$ over the ^{12}C γ spectrum shown in Fig. 2 results in a total transmission of 97.96%. These transmission terms in the integrand of the numerator in Eq. (13) account for the fact that the measured S_γ^{puck} is affected by the puck holder and puck which are directly in the line of sight to TCC. A similar transmission term is applied to the integrand in the denominator of Eq. (13). $t_\gamma^{\text{DT}}(E)$ is the energy-dependent transmission of D-T γ's through the full puck holder and puck. This is also determined from bulk mass attenuation coefficients provided by NIST. The integral of $t_\gamma^{\text{DT}}(E)$ over the D-T γ spectrum results in a total transmission of 97.54%. The ratio $S_\gamma^{\text{DT}}(E_{\text{thr}})/S_\gamma^{\text{puck}}(E_{\text{thr}})$ in Eq. (13) can be expressed in terms of the number of productive Cherenkov photons that comprise each signal. Recall that $S_\gamma^{\text{puck}}(E_{\text{thr}})$ in Fig. 6 results from a background configuration shot subtracted from an active configuration shot. Taking this into consideration, the appropriate expression for the ratio of the signals is given as

$$\frac{S_\gamma^{\text{DT}}(E_{\text{thr}})}{S_\gamma^{\text{puck}}(E_{\text{thr}})} = \frac{N_\gamma^{\text{DT}}}{N_\gamma^{\text{active}} - \frac{Y^{\text{active}}}{Y^{\text{background}}} N_\gamma^{\text{background}}}. \tag{14}$$

N_γ^{DT} represents the number of productive Cherenkov photons that comprise $S_\gamma^{\text{DT}}(E_{\text{thr}})$ and is determined by the integral of the signals shown in Fig. 5 divided by QG (the product of the gain and quantum efficiency of the PMT) and er (the product of the electron charge in Coulombs and the scope input impedance in ohms). Similarly, N_γ^{active} ($N_\gamma^{\text{background}}$) is the number of Cherenkov photons that comprise the signal in the active (background) configuration, bounded by the dot-dashed vertical lines shown in Fig. 4. And Y^{active} ($Y^{\text{background}}$) are the corresponding D-T neutron yields. The denominator on the right of the expression in Eq. (14) then represents the number of photons that comprise $S_\gamma^{\text{puck}}(E_{\text{thr}})$ in Fig. 6.

The SiO_2 capsule target also contributes to the primary γ signal shown in Fig. 5 via inelastic neutron scattering which results in γ-ray production. The expression in Eq. (6) can be rewritten to account for this contamination and is expressed as

$$S_\gamma^{\text{DT+capsule}} = Y_n^{\text{DT}} \times QGer \times \left(\frac{\Delta\Omega_\gamma^{\text{DT}}}{4\pi} \right) \times \int_{E_{\text{thr}}}^{\infty} \left[B_{\frac{\gamma}{n}}^{\text{DT}} I_\gamma^{\text{DT}}(E) + \epsilon I_\gamma^{\text{capsule}}(E) \right] \times R'(E, E_{\text{thr}}) dE. \tag{15}$$

$I_\gamma^{\text{capsule}}(E)$ is the capsule γ spectrum. ϵ depends on the effective areal density (ρR) of the SiO_2 capsule during the implosion as well as the inelastic neutron scattering cross sections for ^{28}Si and ^{16}O ($\sigma_{n\text{Si}}$ and $\sigma_{n\text{O}}$). It is defined as

$$\epsilon = \rho R \times \left(\frac{\langle W t_{\text{frac}} \rangle_{\text{Si}} \sigma_{n\text{Si}}}{m_{\text{Si}}} + \frac{\langle W t_{\text{frac}} \rangle_{\text{O}} \sigma_{n\text{O}}}{m_{\text{O}}} \right). \tag{16}$$

$\langle W t_{\text{frac}} \rangle$ are the weight or mass fractions for Si and O, and m are the corresponding masses for a single atom. ρR was measured in these experiments by the DAD [22]. The resulting average ρR, measured from all of the shots with similar capsule diameter and thickness, is 2.05 ± 0.24 mg/cm^2. For shots 77 361 and 77 374, the active configuration scenarios, the capsule ρR was measured to be 1.69 ± 0.74 and 2.25 ± 0.76 mg/cm^2, respectively. The capsule γ spectrum [$I_\gamma^{\text{capsule}}(E)$] is determined by three independent methods. The first is via Monte Carlo N-particle (MCNP) simulations [46], in which 14.1-MeV neutrons are incident on a SiO_2 shell of a given density. A second method instead relies on GEANT4 simulations [43]. The third method is analytical and relies on nuclear data tables and databases [47–49], for which the inelastic neutron scattering cross section for γ production $(n,n'\gamma)$ is determined from ENDF/B-VIII.0 and JENDL-4.0 databases [50–51]. Scattering to 17 excited levels is considered for both ^{28}Si and ^{16}O. The resulting total cross sections, for 14.1-MeV incident neutrons, are found to be 293.0 $\pm$ 28.8 mb for ^{28}Si and 317.9 $\pm$ 33.4 mb for ^{16}O. The scattering cross section to each excited level and the deexcitation scheme from that level then determine the resulting γ spectrum. A comparison of the resulting analytical spectrum, for SiO_2 with a ρR of 2.05 mg/cm^2, against the MCNP simulations shows similar amplitudes for most of the intense spectral lines. Lower energy spectral features are not captured in the analytical method as Compton scattering and other effects are not considered. For these reasons, the MCNP and GEANT4 simulation results are used to determine the capsule ρR contribution to the primary γ signal. In Fig. 8, both the MCNP (solid, blue) and GEANT4 (dotted, red) simulation results are compared. The choice of database used and other

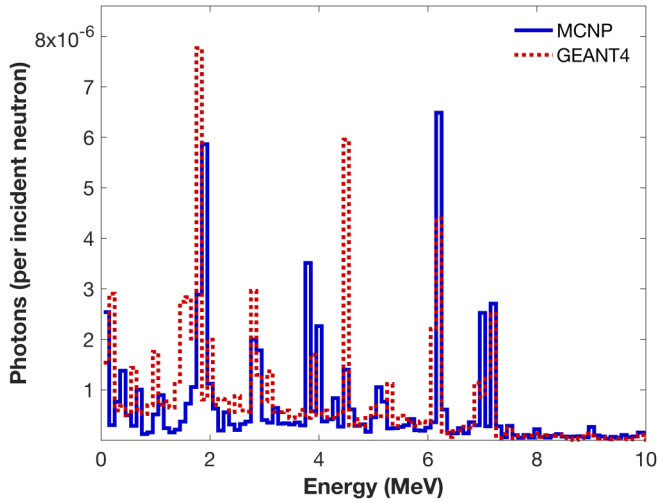

FIG. 8. The SiO_2 capsule spectra are shown for an areal density of 2.05 mg/cm^2. The solid, blue curve represents the spectrum generated from MCNP simulations, and the dotted, red curve represents the spectrum generated from GEANT4 simulations.

techniques that are inherent to each code may result in the noticeable differences between the two generated spectra.

With the capsule γ spectra defined and ρR measurements provided by the DAD, a corrected expression for the D-T (γ/n) branching ratio is found by taking a ratio of the expressions given in Eqs. (12) and (15) and solving for $B^{\mathrm{DT}}_{\frac{\gamma}{n}}$:

$$B^{\mathrm{DT}}_{\frac{\gamma}{n}} = \frac{\Delta\Omega^{\mathrm{puck}}_{\gamma} M_{\mathrm{puck}}}{\Delta\Omega^{\mathrm{DT}}_{\gamma} 4\pi D^2 m_C} \times \sigma_{nC} \times f_1 \times \left\{ \frac{S^{\mathrm{DT}}_{\gamma}(E_{\mathrm{thr}})}{S^{\mathrm{puck}}_{\gamma}(E_{\mathrm{thr}})} \right\} \times \left\{ \frac{\int_{E_{\mathrm{thr}}}^{\infty} t_n^{\mathrm{puck}} t_{\gamma}^{\mathrm{puck}}(E) I_{\gamma}^{\mathrm{puck}}(E) R''(E, E_{\mathrm{thr}}) dE}{\int_{E_E}^{\infty} t_{\gamma}^{\mathrm{DT}}(E) I_{\gamma}^{\mathrm{DT}}(E) R'(E, E_{\mathrm{thr}}) dE} \right\} - \epsilon \times \left\{ \frac{\int_{E_{\mathrm{thr}}}^{\infty} t_{\gamma}^{\mathrm{DT}}(E) I_{\gamma}^{\mathrm{capsule}}(E) R'(E, E_{\mathrm{thr}}) dE}{\int_{E_{\mathrm{thr}}}^{\infty} t_{\gamma}^{\mathrm{DT}}(E) I_{\gamma}^{\mathrm{DT}}(E) R'(E, E_{\mathrm{thr}}) dE} \right\}. \quad (17)$$

The last term in the above expression represents the SiO_2 capsule ρR correction. For the final D-T branching ratio result, this correction term is an average of the MCNP and GEANT4 based simulations.

D. Results

The D-T (γ/n) branching ratio can be calculated for the two shots in the active configuration ($B1^{\mathrm{DT}}_{\frac{\gamma}{n}}$ and $B2^{\mathrm{DT}}_{\frac{\gamma}{n}}$) along with a corresponding variance for each. The total variance is given by

$$\delta B = \sqrt{\left(\frac{\partial B}{\partial X}\delta X\right)^2 + \left(\frac{\partial B}{\partial Y}\delta Y\right)^2 + \ldots}, \quad (18)$$

with X and Y representing particular physical quantities with corresponding variances δX and δY. Table I contains most of the relevant information, with the physical quantities and variances given where appropriate. The first column lists the physical quantity, the second contains its value, the third contains its variance, and the fourth and fifth columns contain its relative contribution to the total variance for each of the two calculated branching ratios. This relative contribution is expressed as $|\frac{\partial B}{\partial X}\delta X|$ for each physical quantity (X).

For the number of productive Cherenkov photons (N_{γ}) that comprise a measured signal [Eq. (14)], the variance is estimated as the square root of the corresponding number of productive electrons ($\sqrt{N_e}$), determined from the GCD-3 response curve such as in Fig. 7. The ^{12}C$(n, n'\gamma)$ ^{12}C γ spectrum is assumed to have no variance because of the intense peak near 4.44 MeV which is orders of magnitude larger than other spectral features. Variations in the other less intense spectral features will have negligible effects on the D-T branching ratio and its total error. It should be noted that there is a correction factor for the GCD-3 responsivity (R', R'') which is calculated in Ref. [40]. The correction factor accounts for transmission and reflectivity losses in the optical components contained in the diagnostic. To first order, this correction is an absolute multiplicative factor, and so cancels in the ratio of integrands in Eq. (17). The variance in the shape of the capsule γ spectrum is not directly accounted for in the total error of the branching ratio. Only the more intense and higher energy spectral features will have a significant effect on the correction to the branching ratio, and these are roughly in agreement for the MCNP and GEANT4 generated spectra. The cross sections for ^{28}Si and ^{16}O are inherent to the MCNP and GEANT4 code, and so the corresponding variances are also not directly incorporated into the total error of the branching ratio. To account for these variances, the deviation between independent results obtained from the two methods is added in quadrature to the total error of the branching ratio.

The statistical variance-weighted average for the D-T branching ratio, according to the two shots in the active configuration, is 4.56×10^{-5}. The statistical error is found to be 0.38×10^{-5}, and a systematic error of 0.45×10^{-5}. The deviation between results obtained independently from MCNP and GEANT4 simulations is 0.04×10^{-5}. The final value for the D-T (γ/n) branching ratio as determined from this paper is $(4.56 \pm 0.58) \times 10^{-5}$.

III. DISCUSSION

The reported branching ratio has a significantly reduced variance compared to a previous ICF based measurement [11–12]. The contributions to the total variance arise from both systematic and statistical errors of relevant physical quantities as shown in Table I. The systematic errors include the ^{12}C$(n, n'\gamma)$ ^{12}C scattering cross section (σ_{nC}) at 90°, the geometrical correction factor applied to it (f_1), the uncertainty in the γ_1:γ_0 ratio (Gr), the SiO_2 capsule areal density (ρR), and the mass of the carbon puck (M_{puck}). Statistical errors include the measured signals (number of productive photons) in the different shot configurations as well as the precision in the D-T fusion neutron yield measurements. While there is an absolute, or systematic, error associated with these nToF based yield measurements, it is not requisite in these circumstances since the expressions in Eqs. (13) and (17) for the D-T (γ/n) branching ratio involve a ratio of neutron yields. Because the ^{12}C γ signal arises from a yield normalized

TABLE I. Relevant physical quantities are listed (first column) along with their value and variance when applicable (second and third columns). Also listed for each physical quantity are the relative contributions to the total variance in the calculated branching ratios $B1^{\rm DT}_{\frac{\gamma}{n}}$ and $B2^{\rm DT}_{\frac{\gamma}{n}}$ (fourth and fifth columns).

Quantity	Value	Variance	$\left\vert\frac{\partial B1}{\partial X}\delta X\right\vert$	$\left\vert\frac{\partial B2}{\partial X}\delta X\right\vert$
Gr	2.1	0.4	7.83×10^{-7}	8.50×10^{-7}
$\sigma_{n\rm C}$ (mb)	153.8	3.9	1.25×10^{-6}	1.39×10^{-6}
f_1	1.369	0.089	3.21×10^{-6}	3.57×10^{-6}
$M_{\rm puck}$ (g)	5.93	0.1	8.32×10^{-7}	9.26×10^{-7}
ρR_1 (mg/cm^2)	1.69	0.74	2.32×10^{-6}	
ρR_2 (mg/cm^2)	2.25	0.76		2.38×10^{-6}
$\sigma_{n\rm Si}$ (mb)	293.0	28.85		
$\sigma_{n\rm O}$ (mb)	317.9	33.38		
$Y^{\rm active-1}$	9.87×10^{13}	7.73×10^{11}	3.50×10^{-6}	
$Y^{\rm active-2}$	9.27×10^{13}	7.27×10^{11}		4.17×10^{-6}
$Y^{\rm background}$	9.54×10^{13}	7.47×10^{11}	3.50×10^{-6}	4.16×10^{-6}
$N_\gamma^{\rm DT-1}$	7.01×10^{6}	1.96×10^{4}	1.38×10^{-7}	
$N_\gamma^{\rm DT-2}$	6.86×10^{6}	1.94×10^{4}		1.56×10^{-7}
$N_\gamma^{\rm carbon-1}$	1.63×10^{6}	6.41×10^{3}	1.94×10^{-7}	
$N_\gamma^{\rm carbon-2}$	1.44×10^{6}	6.01×10^{3}		2.30×10^{-7}
$B1^{\rm DT}_{\frac{\gamma}{n}}$	4.41×10^{-5}	6.57×10^{-6}	1	
$B2^{\rm DT}_{\frac{\gamma}{n}}$	4.79×10^{-5}	7.53×10^{-6}		1

subtraction of the background configuration signal from the active configuration, the relatively small precision errors in the neutron yield measurements have a significant impact on the total D-T branching ratio variance. The statistical variance in the measured signals is negligible.

The reported D-T (γ/n) branching ratio and its total variance are compared to results obtained from previous experiments [11–12,25–27,29,31], both ICF and accelerator based. Beam-target experiments typically utilize a range of deuteron beam energies. In ICF plasmas at thermal equilibrium, most of the nuclear reactions occur at the Gamow peak energy (E_0). For a D-T reaction, the Gamow peak energy can be expressed as $E_0 = 6.66(T_{\rm ion})^{2/3}$ in a center-of-mass reference [16,52]. Here $T_{\rm ion}$ is the burn-averaged ion temperature in keV and is equal to 10.3 ± 0.8 for the shots relevant to this paper. For the ICF based experiments, the resulting E_0 is translated into an effective deuteron beam energy. All experimental results [11–12,25–27,29,31], including the corresponding variances, are shown in Fig. 9 as a function of the (effective) deuteron beam energy. The results obtained in this paper (black square) as well as in Refs. [11,12] (red square) are ICF based measurements which consider both the γ_1 and γ_0 components of the D-T γ spectrum. The experiments conducted in Refs. [27,29,31] (yellow, blue, and cyan solid circles, respectively) are beam-target based experiments which also consider both the γ_1 and γ_0 components. And finally, the experiments conducted in Refs. [25–26] (magenta and green open circles, respectively) are beam-target experiments that only consider the γ_0 component of the D-T γ spectrum. There is significant discrepancy in these results. $B^{\rm DT}_{\gamma/n}$ is a relatively small quantity. Detection of the γ's is further complicated due to neutron scattering and the potential noise created from $(n, n'\gamma)$ interactions. These results suggest that more measurements are necessary, both accelerator and ICF based, with reduced statistical and systematic uncertainties.

The D-T (γ/n) branching ratio, as determined from experiments conducted at the OMEGA laser facility and utilizing the

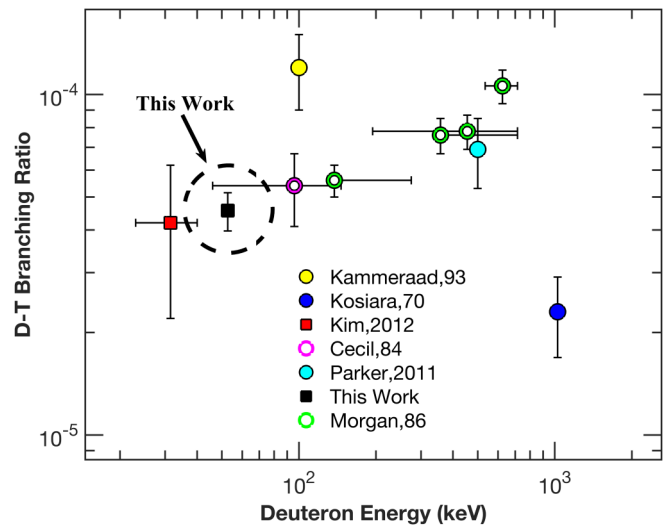

FIG. 9. The results of several experiments to measure the D-T (γ/n) branching ratio are shown. The branching ratio is plotted against the (effective) deuteron energy. The squares represent ICF based measurements which consider both the γ_1 and γ_0 components of the D-T γ spectrum. The solid circles represent beam-target experiments which also consider both the γ_1 and γ_0 components. And the open circles represent beam-target experiments which only consider the γ_0 component of the D-T γ spectrum.

GCD-3 equipped with a ^{12}C puck, is reported here. Mitigation of background noise over previous beam-target experiments, a cross-calibration to the inelastic neutron scattering cross section in ^{12}C [^{12}C$(n, n'\gamma)$ ^{12}C], and an improved understanding of the D-T fusion γ spectrum all contribute to significantly reduced uncertainties in the branching ratio. This paper builds upon a unique puck-based determination of this fundamental nuclear property. It asserts the use of ICF implosion plasmas as a platform to study nuclear physics and provide precision measurements to augment traditional accelerator-based methods.

Several improvements can be made for an ICF based cross-calibration of the D-T (γ/n) branching ratio. The individual errors associated with some of the relevant quantities, which have a significant contribution to the total variance, can be further reduced. A modern measurement of the ^{12}C$(n, n'\gamma)$ ^{12}C differential scattering cross section could be beneficial in reducing the error in $\sigma_{n\mathrm{C}}$. Instead of using a ^{12}C disc, an annulus could be used. This can reduce the error in the effective geometrical correction factor (f_1). To reduce the effects of the precision errors in Y^{active} and $Y^{\mathrm{background}}$, the puck-to-TCC and GCD-3-to-TCC distances can be optimized to temporally separate the ^{12}C γ signal from the extraneous neutron induced signal. The GCD-3 can also be operated at different thresholds to experimentally constrain the ^{28}Si and ^{16}O cross sections. Additional shot data would further reduce statistical errors, while the use of materials other than ^{12}C could potentially reduce systematic errors. Ideally, ϵ defined in Eq. (16) is zero or negligible. This can be achieved by using thinner target capsules to reduce ρR, and possibly with the use of a different capsule material. Future experiments will be conducted that will incorporate these modifications.

ACKNOWLEDGMENTS

We thank the operations crews and engineering staff at OMEGA for supporting these experiments. This work was performed under the auspices of the U.S. Department of Energy (DOE) by Lawrence Livermore National Laboratory in part under Contract No. DE-AC52-07NA27344 and supported by the U.S. DOE Early Career Research Program (Fusion Energy Sciences) under Grant No. FWP SCW1658; and by the Los Alamos National Laboratory, operated by Triad National Security, LLC for the National Nuclear Security Administration of the U.S. DOE under Contract No. 89233218CNA000001. LLNL-JRNL-823874.

[1] H.-S. Bosch and G. M. Hale, Improved formulas for fusion cross-sections and thermal reactivities, Nucl. Fusion. **32**, 611 (1992).

[2] P. Navrátil and S. Quaglioni, *Ab Initio* Many-Body Calculations of the ^{3}H(d, n) ^{4}He and ^{4}He(d, p) ^{4}He Fusion Reactions, Phys. Rev. Lett. **108**, 042503 (2012).

[3] L. Bertalot, V. Krasilnikov, L. Core, A. Saxena, N. Yukhnov, R. Barnsley, and M. Walsh, Present status of ITER neutron diagnostics development, J. Fusion Energy **38**, 283 (2019).

[4] M. Salewski, M. Nocente, A. S. Jacobsen, F. Binda, C. Cazzaniga, G. Ericsson, J. Eriksson, G. Gorini, C. Hellesen, A. Hjalmarsson, V. G. Kiptily, T. Koskela, S. B. Korsholm, T. Kurki-Suonio, F. Leipold, J. Madsen, D. Moseev, S. K. Nielsen, J. Rasmussen, M. Schneider, S. E. Sharapov, M. Stejner, M. Tardocchi, and J. E. T. Contributors, MeV-range velocity-space tomography from gamma-ray and neutron emission spectrometry measurements at JET, Nucl. Fusion. **57**, 056001 (2017).

[5] J. Nuckolls, L. Wood, A. Thiessen, and G. Zimmerman, Laser compression of matter to super-high densities: Thermonuclear (CTR) applications, Nature (London) **239**, 139 (1972).

[6] T. R. Boehly, D. L. Brown, R. S. Craxton, R. L. Keck, J. P. Knauer, J. H. Kelly, T. J. Kessler, S. A. Kumpan, S. J. Loucks, S. A. Letzring, F. J. Marshall, R. L. McCrory, S. F. B. Morse, W. Seka, J. M. Sources, and C. P. Verdon, Initial performance results of the OMEGA laser system, Optics Communications **133**, 495 (1997).

[7] D. H. Munro, J. E. Field, R. Hatarik, J. L. Peterson, E. P. Hartouni, B. K. Spears, and J. D. Kilkenny, Impact of temperature-velocity distribution on fusion neutron peak shape, Phys. Plasmas **24**, 056301 (2017).

[8] Brian K. Spears, M. J. Edwards, S. Hatchett, J. Kilkenny, J. Knauer, A. Kritcher, J. Lindl, D. Munro, P. Patel, H. F. Robey, and R. P. J. Town, Mode 1 drive asymmetry in inertial confinement fusion implosions on the National Ignition Facility, Phys. Plasmas **21**, 042702 (2014).

[9] H. W. Herrmann, J. M. Mack, C. S. Young, R. M. Malone, W. Stoeffl, and C. J. Horsfield, Cherenkov radiation conversion and collection considerations for a gamma bang time/reaction history diagnostic for the NIF, Rev. Sci. Instrum. **79**, 10E531 (2008).

[10] A. J. Crilly, B. D. Appelbe, O. M. Mannion, C. J. Forrest, V. Gopalaswamy, C. A. Walsh, and J. P. Chittenden, Neutron backscatter edge: A measure of the hydrodynamic properties of the dense DT fuel at stagnation in ICF experiments, Phys. Plasmas **27**, 012701 (2020).

[11] Y. Kim, J. M. Mack, H. W. Herrmann, C. S. Young, G. M. Hale, S. Caldwell, N. M. Hoffman, S. C. Evans, T. J. Sedillo, A. McEvoy, J. Langenbrunner, H. H. Hsu, M. A. Huff, S. Batha, C. J. Horsfield, M. S. Rubery, W. J. Garbett, W. Stoeffl, E. Grafil, L. Bernstein, J. A. Church, D. B. Sayre, M. J. Rosenberg, C. Waugh, H. G. Rinderknecht, M. Gatu Johnson, A. B. Zylstra, J. A. Frenje, D. T. Casey, R. D. Petrasso, E. Kirk Miller, V. Yu Glebov, C. Stoeckl, and T. C. Sangster, D-T gamma-to-neutron branching ratio determined from inertial confinement fusion plasmas, Phys. Plasmas **19**, 056313 (2012).

[12] Y. Kim, J. M. Mack, H. W. Herrmann, C. S. Young, G. M. Hale, S. Caldwell, N. M. Hoffman, S. C. Evans, T. J. Sedillo, A. McEvoy, J. Langenbrunner, H. H. Hsu, M. A. Huff, S. Batha, C. J. Horsfield, M. S. Rubery, W. J. Garbett, W. Stoeffl, E. Grafil, L. Bernstein, J. A. Church, D. B. Sayre, M. J. Rosenberg, C. Waugh, H. G. Rinderknecht, M. Gatu Johnson, A. B. Zylstra, J. A. Frenje, D. T. Casey, R. D. Petrasso, E. Kirk Miller, V. Yu Glebov, C. Stoeckl, and T. C. Sangster, Determination of the deuterium-tritium branching ratio based on inertial confinement fusion implosions, Phys. Rev. C **85**, 061601(R) (2012).

[13] A. B. Zylstra, H. W. Herrmann, M. Gatu Johnson, Y. H. Kim, J. A. Frenje, G. Hale, C. K. Li, M. Rubery, M. Paris, A. Bacher, C. R. Brune, C. Forrest, V. Yu. Glebov, R. Janezic, D. McNabb, A. Nikroo, J. Pino, T. C. Sangster, F. H. Séguin, W. Seka, H. Sio, C. Stoeckl, and R. D. Petrasso, Using Inertial Fusion Implosions to Measure the T + ^{3}He Fusion Cross Section at Nucleosynthesis-Relevant Energies, Phys. Rev. Lett. **117**, 035002 (2016).

[14] A. B. Zylstra, H. W. Herrmann, Y. H. Kim, A. McEvoy, J. A. Frenje, M. Gatu Johnson, R. D. Petrasso, V. Yu. Glebov, C. Forrest, J. Delettrez, S. Gales, and M. Rubery, ^{2}H(p,γ) ^{3}He cross section measurement using high-energy-density plasmas, Phys. Rev. C **101**, 042802(R) (2020).

[15] D. T. Casey, D. B. Sayre, C. R. Brune, V. A. Smalyuk, C. R. Weber, R. E. Tipton, J. E. Pino, G. P. Grim, B. A. Remington, D. Dearborn, L. R. Benedetti, J. A. Frenje, M. Gatu-Johnson, R. Hatarik, N. Izumi, J. M. McNaney, T. Ma, G. A. Kyrala, S. MacLaren, J. Salmonson, S. F. Khan, A. Pak, L. Berzak Hopkins, S. LePape, B. K. Spears, N. B. Meezan, L. Divol, C. B. Yeamans, J. A. Caggiano, D. P. McNabb, D. M. Holunga, M. Chiarappa-Zucca, T. R. Kohut, and T. G. Parham**,** Thermonuclear reactions probed at stellar-core conditions with laser-based inertial-confinement fusion, Nat. Phys. **13**, 1227 (2017).

[16] S. Atzeni, Laser driven inertial fusion: The physical basis of current and recently proposed ignition experiments, Plasma Phys. Control. Fusion **51**, 124029 (2009).

[17] N. M. Hoffman, D. C. Wilson, H. W. Herrmann, and C. S. Young, Using gamma-ray emission to measure areal density of inertial confinement fusion capsules, Rev. Sci. Instrum. **81**, 10D333 (2010).

[18] D. C. Wilson, P. A. Bradley, C. J. Cerjan, J. D. Salmonson, B. K. Spears, S. P. Hatchet II, H. W. Herrmann, and V. Yu. Glebov, Diagnosing ignition with DT reaction history**,** Rev. Sci. Instrum. **79**, 10E525 (2008).

[19] G. Beck, Contribution to the theory of the Cherenkov effect, Phys. Rev. **74**, 795 (1948).

[20] D. J. Schlossberg, A. S. Moore, B. V. Beeman, M. J. Eckart, G. P. Grim, E. P. Hartouni, R. Hatarik, M. S. Rubery, D. B. Sayre, and C. Waltz, *Ab initio* response functions for Cherenkov-based neutron detectors, Rev. Sci. Instrum. **89**, 10I136 (2018).

[21] A. S. Moore, D. J. Schlossberg, E. P. Hartouni, D. Sayre, M. J. Eckart, R. Hatarik, F. Barbosa, J. Root, C. Waltz, B. Beeman, M. S. Rubery, and G. P. Grim, A fused silica Cherenkov radiator for high precision time-of-flight measurement of DT γ and neutron spectra, Rev. Sci. Instrum. **89**, 10I120 (2018).

[22] M. S. Rubery, C. J. Horsfield, S. G. Gales, W. J. Garbett, A. Leatherland, C. Young, H. Herrmann, Y. Kim, N. M. Hoffman, J. M. Mack, R. Aragonez, T. Sedillo, S. Evans, R. B. Brannon, C. Stoeckl, J. Ulreich, A. Sorce, G. Gates, M. J. Shoup, III, B. Peck, M. Gatu Johnson, J. A. Frenje, J. S. Milnes, and W. Stoeffl, First measurements of remaining shell areal density on the OMEGA laser using the diagnostic for areal density (DAD), Rev. Sci. Instrum. **89**, 083510 (2018).

[23] J. M. Mack, R. R. Berggren, S. E. Caldwell, S. C. Evans, J. R. Faulkner, Jr., R. A. Lerche, J. A. Oertel, and C. S. Young, Observation of high-energy deuterium–tritium fusion gamma rays using gas Cherenkov detectors, Nucl. Instrum. Methods Phys. Res., Sect. A **513**, 566 (2003).

[24] H. W. Herrmann, Y. H. Kim, C. S. Young, V. E. Fatherley, F. E. Lopez, J. A. Oertel, R. M. Malone, M. S. Rubery, C. J. Horsfield, W. Stoeffl, A. B. Zylstra, W. T. Shmayda, and S. H. Batha, Extended performance gas Cherenkov detector for gamma-ray detection in high-energy density experiments, Rev. Sci. Instrum. **85**, 11E124 (2014).

[25] F. E. Cecil and F. J. Wilkinson, III, Measurement of the Ground-State Gamma-Ray Branching Ratio of the DT Reaction at Low Energies, Phys. Rev. Lett. **53**, 767 (1984).

[26] G. L. Morgan, P. W. Lisowski, S. A. Wender, R. E. Brown, N. Jarmie, J. F. Wilkerson, and D. M. Drake, Measurement of the branching ratio ^{3}H$(d,\gamma)/\,^3$H(d,n) using thick tritium gas targets, Phys. Rev. C **33**, 1224 (1986).

[27] J. E. Kammeraad, J. Hall, K. E. Sale, C. A. Barnes, S. E. Kellogg, and T. R. Wang, Measurement of the cross-section ratio ^{3}H(d,γ) ^{5}He / ^{3}H$(d,\alpha)n$ at 100 keV, Phys. Rev. C **47**, 29 (1993).

[28] W. Buss, H. Waffler, and B. Ziegler, Radiative capture of deuterons by H^3, Phys. Lett. **4**, 198 (1963).

[29] A. Kosiara and H. B. Willard, Gamma ray-neutron branching ratio in the triton-deuteron reaction, Phys. Lett. B **32**, 99 (1970).

[30] M. J. Balbes, J. C. Riley, G. Feldman, H. R. Weller, and D. R. Tilley, Polarized deuteron capture by ^{3}He and ^{3}H at and above the fusion resonance region, Phys. Rev. C **49**, 912 (1994).

[31] C. E. Parker, The ^{3}H(d,γ) Reaction and the ^{3}H$(d,\gamma)/\,^3$H(d,n) Branching Ratio for $E_{c.m.} \leqslant 300\ keV$, Ph.D. thesis, Ohio University, 2016.

[32] C. E. Parker, C. R. Brune, T. N. Massey, J. E. O'Donnell, A. L. Richard, and D. B. Sayre, The ^{3}H(d,γ) ^{5}He reaction for $E_{\text{c.m.}} \leqslant 300$ keV, EPJ Web Conf. **113**, 03005 (2016).

[33] C. J. Horsfield, M. S. Rubery, J. M. Mack, H. W. Herrmann, Y. Kim, C. S. Young, S. E. Caldwell, S. C. Evans, T. S. Sedillo, A. M. McEvoy, N. M. Hoffman, M. A. Huff, J. R. Langenbrunner, G. M. Hale, D. C. Wilson, W. Stoeffl, J. A. Church, E. M. Grafil, E. K. Miller, and V. Yu Glebov, First spectral measurement of deuterium-tritium fusion γ rays in inertial fusion experiments, Phys. Rev. C **104**, 024610 (2021).

[34] D. T. Casey, J. A. Frenje, M. Gatu Johnson, F. H. Séguin, C. K. Li, R. D. Petrasso, V. Yu. Glebov, J. Katz, J. Magoon, D. D. Meyerhofer, T. C. Sangster, M. Shoup, J. Ulreich, R. C. Ashabranner, R. M. Bionta, A. C. Carpenter, B. Felker, H. Y. Khater, S. LePape, A. MacKinnon, M. A. McKernan, M. Moran, J. R. Rygg, M. F. Yeoman, R. Zacharias, R. J. Leeper, K. Fletcher, M. Farrell, D. Jasion, J. Kilkenny, and R. Paguio, The magnetic recoil spectrometer for measurements of the absolute neutron spectrum at OMEGA and the NIF, Rev. Sci. Instrum. **84**, 043506 (2013).

[35] D. L. Bleuel, C. B. Yeamans, L. A. Bernstein, R. M. Bionta, J. A. Caggiano, D. T. Casey, G. W. Cooper, O. B. Drury, J. A. Frenje, C. A. Hagmann, R. Hatarik, J. P. Knauer, M. Gatu Johnson, K. M. Knittel, R. J. Leeper, J. M. McNaney, M. Moran, C. L. Ruiz, and D. H. G. Schneider, Neutron activation diagnostics at the National Ignition Facility, Rev. Sci. Instrum. **83**, 10D313 (2012).

[36] M. E. Battat and E. R. Graves, Gamma rays from 14-Mev neutron bombardment of C^{12}, Phys. Rev. **97**, 1266 (1955).

[37] J. Benveniste, A. C. Mitchell, C. D. Schrader, and J. H. Zenger, Gamma rays from the interaction of 14-MeV neutrons with carbon, Nucl. Phys. **19**, 448 (1960).

[38] J. D. Anderson, C. C. Gardner, J. W. McClure, M. P. Nakada, and C. Wong, Inelastic scattering of 14-Mev neutrons from carbon and beryllium, Phys. Rev. **111**, 572 (1958).

[39] D. Spaargaren and C. C. Jonker, Angular correlations in inelastic neutron scattering by carbon at 15.0 MeV, Nucl. Phys. A. **161**, 354 (1971).

[40] A. B. Zylstra, H. W. Herrmann, Y. H. Kim, A. McEvoy, K. Meaney, V. Yu. Glebov, and M. Rubery, Improved calibration of the OMEGA gas Cherenkov detector, Rev. Sci. Instrum. **90**, 123504 (2019).

[41] A. M. McEvoy, H. W. Herrmann, Y. Kim, T. S. Sedillo, H. Geppert- Kleinrath, C. R. Brune, T. N. Massey, A. V. Voinov, C. E. Parker, M. S. Rubery, and W. Stoeffl, ^{13}C$(n, 2n\gamma)$ ^{12}C γ-ray production in the 14–16 MeV incident neutron energy range, Phys. Rev. C **103**, 064607 (2021).

[42] G. M. Hale, Use of *R*-matrix theory in light element evaluations, Los Alamos National Laboratory Report No. LA-UR-93-102, 1993 (unpublished).

[43] J. Allison, K. Amako, J. Apostolakis, P. Arce, M. Asai, T. Aso, E. Bagli, A. Bagulya, S. Banerjee, G. Barrand, B. R. Beck, A. G. Bogdanov, D. Brandt, J. M. C. Brown, H. Burkhardt, Ph. Canal, D. Cano-Ott, S. Chauvie, K. Cho, G. A. P. Cirrone, G. Cooperman, M. A. Cortés-Giraldo, G. Cosmo, G. Cuttone, G. Depaola, L. Desorgher, X. Dong, A. Dotti, V. D. Elvira, G. Folger, Z. Francis, A. Galoyan, L. Garnier, M. Gayer, K. L. Genser, V. M. Grichine, S. Guatelli, P. Gueye, P. Gumplinger, A. S. Howard, I. Hrivnacova, S. Hwang, S. Incerti, A. Ivanchenko, V. N. Ivanchenko, F. W. Jones, S. Y. Jun, P. Kaitaniemi, N. Karakatsanis, M. Karamitros, M. Kelsey, A. Kimura, T. Koi, H. Kurashige, A. Lechner, S. B. Lee, F. Longo, M. Maire, D. Mancusi, A. Mantero, E. Mendoza, B. Morgan, K. Murakami, T. Nikitina, L. Pandola, P. Paprocki, J. Perl, I. Petrovic, M. G. Pia, W. Pokorski, J. M. Quesada, M. Raine, M. A. Reis, A. Ribon, A. Ristic Fira, F. Romano, G. Russo, G. Santin, T. Sasaki, D. Sawkey, J. I. Shin, I. I. Strakovsky, A. Taborda, S. Tanaka, B. Tome, T. Toshito, H. N. Tran, P. R. Truscott, L. Urban, V. Uzhinsky, J. M. Verbeke, M. Verderi, B. L. Wendt, H. Wenzel, D. H. Wright, D. M. Wright, T. Yamashita, J. Yarba, and H. Yoshida, Recent developments in GEANT4, Nucl. Instrum. Methods Phys. Res., Sect. A **835**, 186 (2016).

[44] N. M. Hoffman, H. W. Herrmann, Y. H. Kim, H. H. Hsu, C. J. Horsfield, M. S. Rubery, D. C. Wilson, W. Stoeffl, C. S. Young, J. M. Mack, E. K. Miller, E. Grafil, S. C. Evans, T. J. Sedillo, V. Yu. Glebov, and T. Duffy, *In situ* calibration of the Gamma Reaction History instrument using reference samples ("pucks") for areal density measurements, EPJ Web Conf. **59**, 13019 (2013).

[45] J. H. Hubbell, Experimentally measured total x-ray attenuation coefficients extracted from previously unprocessed documents held by the NIST photon and charged particle data center, NIST Interagency/Internal Report (NISTIR) (1996).

[46] R. A. Forster, L. J. Cox, R. F. Barrett, T. E. Booth, J. F. Briesmeister, F. B. Brown, J. S. Bull, G. C. Geisler, J. T. Goorley, R. D. Mosteller, S. E. Post, R. E. Prael, E. C. Selcow, and A. Sood, MCNP version 5, Nucl. Instr. and Meth. in Phys. Res. B **213**, 82 (2004).

[47] A. A. Sonzogni, NuDat 2.0: Nuclear structure and decay data on the internet, AIP Conf. Proc. **769**, 574 (2005).

[48] N. Soppera, M. Bossant, and E. Dupont, JANIS 4: An improved version of the NEA Java-based nuclear data information system, Nucl. Data Sheets **120**, 294 (2014).

[49] R. B. Firestone, S. Y. F. Chu, and C. M. Baglin, *Table of Isotopes: 1999 Update*, 8th ed. (Wiley, New York, 1999).

[50] D. A. Brown, M. B. Chadwick, R. Capote, A. C. Kahler, A. Trkov, M. W. Herman, A. A. Sonzogni, Y. Danon, A. D. Carlson, M. Dunn, D. L. Smith, G. M. Hale, G. Arbanas, R. Arcilla, C. R. Bates, B. Beck, B. Becker, F. Brown, R. J. Casperson, J. Conlin, D. E. Cullen, M.-A. Descalle, R. Firestone, T. Gaines, K. H. Guber, A. I. Hawari, J. Holmes, T. D. Johnson, T. Kawano, B. C. Kiedrowski, A. J. Koning, S. Kopecky, L. Leal, J. P. Lestone, C. Lubitz, J. I. Marquez Damian, C. M. Mattoon, E. A. McCutchan, S. Mughabghab, P. Navratil, D. Neudecker, G. P. A. Nobre, G. Noguere, M. Paris, M. T. Pigni, A. J. Plompen, B. Pritychenko, V. G. Pronyaev, D. Roubtsov, D. Rochman, P. Romano, P. Schillebeeckx, S. Simakov, M. Sin, I. Sirakov, B. Sleaford, V. Sobes, E. S. Soukhovitskii, I. Stetcu, P. Talou, I. Thompson, S. van der Marck, L. Welser-Sherrill, D. Wiarda, M. White, J. L. Wormald, R. Q. Wright, M. Zerkle, and Y. Zhu, ENDF/B-VIII.0: The 8$^{\text{th}}$ major release of the Nuclear Reaction Data Library with CIELO-project cross sections, new standards and thermal scattering data, Nucl. Data Sheets **148**, 1 (2018).

[51] K. Shibata, O. Iwamoto, T. Nakagawa, N. Iwamoto, A. Ichihara, S. Kunieda, S. Chiba, K. Furutaka, N. Otuka, T. Ohsawa, T. Murata, H. Matsunobu, A. Zukeran, S. Kamada, and J. Katakura, JENDL-4.0: A new library for nuclear science and engineering, J. Nucl. Sci. Tech. **48**, 1 (2011).

[52] D. T. Casey, Diagnosing Inertial Confinement Fusion Implosions at OMEGA and the NIF Using Novel Neutron Spectrometry, Ph.D. thesis, Massachusetts Institute of Technology, 2012.